J. Non-Newtonian Fluid Mech. 159 (2009) 1–9

Contents lists available at ScienceDirect

Journal of Non-Newtonian Fluid Mechanics

journal homepage: www.elsevier.com/locate/jnnfm

Stability of the annular Poiseuille flow of a Newtonian liquid with slip along the walls

Maria Chatzimina[a], Georgios C. Georgiou[a,*], Kostas Housiadas[b], Savvas G. Hatzikiriakos[c]

[a] Department of Mathematics and Statistics, University of Cyprus, P.O. Box 20537, 1678 Nicosia, Cyprus
[b] Department of Mathematics, The University of the Aegean, Karlovasi, Samos 83200, Greece
[c] Department of Chemical Engineering, The University of British Columbia, 2216 Main Mall, Vancouver, BC V6T-1Z4, Canada

ARTICLE INFO

Article history:
Received 1 August 2008
Received in revised form
20 September 2008
Accepted 30 October 2008

Keywords:
Newtonian flow
Poiseuille flow
Annulus
Annular extrusion
Slip
Flow curve
Stability

ABSTRACT

The annular Poiseuille flow a Newtonian fluid is studied assuming that slip occurs along the walls. Different slip models relating the wall shear stress to the slip velocity are employed. In the case of non-monotonic slip models with a maximum followed by a minimum, there exist linearly unstable steady-state solutions with one or both the slip velocities along the inner and outer cylinders of the annulus corresponding to the (unstable) negative-slope branch of the slip equation. The resulting flow curve is non-monotonic with one or even two narrow unstable branches corresponding to the stick–slip instability regime. The sizes of these two unstable regimes are reduced as the radii ratio is reduced. It is demonstrated that the second unstable branch may not be observed at all due to the presence of stable steady-states. These results provide a partial explanation for the absence of the stick–slip instability in annular extrusion experiments.

1. Introduction

Among the class of melt fracture extrusion instabilities, the stick–slip instability (or oscillating melt fracture) is the only one that is associated with pressure and extrudate flow-rate oscillations, observed while the throughput is controlled. These oscillations result in extrudate surfaces that are characterized by alternating rough and relatively smooth regions [1]. In general, the stick–slip instability is observed with linear high-molecular weight and narrow-distributed polymers (see [1] and references therein) at apparent shear rates above the sharkskin instability regime and below the gross melt fracture regime [2]. Most of the stick–slip instability experimental studies are performed by using capillary dies with the exception of studies that make use of slits to perform local velocity measurements [3,4]. No systematic observations have been reported on the occurrence of the stick–slip instability in annular dies. However, most important industrial dies utilize this particular form in several applications, including film blowing, blow moulding, wire coating, and pipe production. It is thus clear that further studies are needed to identify under which conditions the stick–slip instability is obtained in annular extrusion.

Rosenbaum [5] and Rosenbaum et al. [6] have reported experimental data for a linear metallocene PE in capillary extrusion and identified clearly the occurrence of stick–slip instability. However, their data for a crosshead die (annular die) showed a continuous flow curve with no stick–slip region. More recently, Delgadillo-Velasquez et al. [7] studied the stick–slip extrusion instability by using several capillary, slit and annular dies and identifying the origin of the different behavior of linear polymers in different geometries with regard to sharkskin and stick–slip instabilities. They reported that while sharkskin and stick–slip instabilities occur in capillary and slit extrusion, they are absent at high ratios of the inside-to-outside diameter of the annular die. They also found that the lack of an observable stick–slip flow regime with annular die flow is due to an inherent difference in the converging flow section in the entrance region of the die when compared to the slip and capillary die geometries. Delgadillo-Velasquez et al. [7] explained these phenomena in terms of the surface-to-volume ratio of the extrudates which is high when sharkskin and stick–slip are absent.

A nice review of numerical studies of steady extrusion from annular dies is provided in the recent paper by Karapetsas and Tsamopoulos [8]. In these studies, emphasis is given on the effects of the constitutive equation and geometry on the thickness and the swelling ratios of the annular extrudate [8–10]. The objective of the present work is to further investigate the origin of the different behavior of linear polymers in annular dies as far as stick–slip

* Corresponding author. Tel.: +357 22892208; fax: +357 22339061.
E-mail address: georgios@ucy.ac.cy (G.C. Georgiou).

0377-0257/$ – see front matter © 2008 Elsevier B.V. All rights reserved.
doi:10.1016/j.jnnfm.2008.10.008

instability is concerned, and to study the effects of both linear and non-monotonic slip and the diameter ratio on the flow curves obtained in annular extrusion. The flow curve is defined as the log–log plot of the wall shear stress versus the apparent wall shear rate, or, equivalently, as the log–log plot of the pressure drop versus the volumetric flow-rate.

The role of slip in polymer extrusion instabilities is well established, especially for the stick–slip instability [2,11]. To our knowledge, there are no reports in the literature concerning the effect of slip on annular extrusion. The theoretical explanations suggested in the literature for the stick–slip instability are based on the non-monotonicity of the flow curve, which exhibits a maximum and a minimum, and the fact that steady-state solutions corresponding to the negative slope regime are linearly unstable [12]. These unstable solutions are thus not encountered in practice; pressure and flow-rate oscillations are observed instead [1,12–14]. Hence, the negative-slope regime of the flow curve corresponds to the stick–slip instability. The transitions from the maximum of the flow curve to the right positive-slope branch and from the minimum to the left positive-slope branch lead to a hysteresis cycle, which is used to describe the observed sudden flow-rate changes in pressure-controlled experiments and the pressure and flow-rate oscillations in flow-rate-controlled ones [2]. The non-monotonicity of the flow curve can be achieved by using non-monotonic slip laws. Such laws relating the wall shear stress to the slip velocity and exhibiting a maximum followed by a minimum, have been proposed for polymer melts by El Kissi and Piau [15] and Adewale and Leonov [16]. Piau and El Kissi [17] also proposed a slip equation with two maxima and two minima for LLDPEs and PBs.

The compressibility/slip mechanism has been the most popular explanation for the stick–slip instability, and is the only one which is consistent with experimental observations. According to this mechanism, the periodic transitions between weak and strong slip at the capillary wall (i.e., the jumps between the two branches of the flow curve), which lead to the pressure and flow-rate oscillations and generate waves on the extrudate surface, are sustained by the compressibility of the melt in the reservoir. This is the mechanism employed in many one-dimensional phenomenological models for the stick–slip instability (see [18] and references therein) and in two-dimensional finite-element simulations of the extrusion process [19].

A full description of the Newtonian annular Poiseuille flow with slip along the wall and the governing equations are presented in Section 2. Three types of slip equations relating the wall shear stress to the slip velocity are considered: (a) a linear (monotonic) slip equation; (b) a non-monotonic piecewise linear slip equation with a maximum and a minimum; and (c) a non-monotonic three-branch slip equation consistent with experimental observations. The numerical results for non-monotonic slip equations are presented and discussed in Section 3. The resulting flow curves indicate that the stick–slip instability regime is shifted to the right and its size is reduced as the radii ratio is reduced. This result may, at least up to some degree, explain the absence of the stick–slip instability in annular extrusion. Our results are summarized in Section 4.

2. One-dimensional annular Poiseuille flow with slip

We consider the one-dimensional steady-state Poiseuille flow of a Newtonian fluid in an annulus of radii κR and R, with $0 < \kappa < 1$, as shown in Fig. 1. It is assumed that slip occurs along the walls following a general slip equation relating the magnitude of the wall shear stress, τ_w, to the slip velocity, u_w:

$$\tau_w = F(u_w) \tag{1}$$

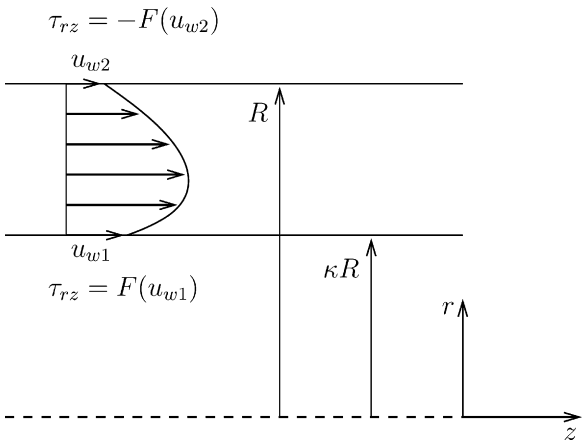

Fig. 1. Geometry and boundary conditions for the annular Poiseuille flow with slip along the walls.

where F is a known function. Due to the fact that the wall shear stresses at the inner and outer cylinders are not the same, the slip velocities along the two walls are not equal. Let us denote the slip velocities along the inner and outer walls by u_{w1} and u_{w2}, respectively. It is a simple exercise to show that the axial velocity u_z and the shear stress τ_{rz} are given by the following general expressions:

$$u_z(r) = u_{w2} - \frac{u_{w1} - u_{w2}}{\ln(1/\kappa)} \ln\frac{r}{R} + \frac{1}{4\eta}\left(-\frac{\partial p}{\partial z}\right) R^2 \left[1 - \left(\frac{r}{R}\right)^2 + \frac{1-\kappa^2}{\ln(1/\kappa)} \ln\frac{r}{R}\right] \tag{2}$$

and

$$\tau_{rz}(r) = -\frac{1}{2}\left(-\frac{\partial p}{\partial z}\right) r + \eta \left[\frac{1}{4\eta}\frac{1-\kappa^2}{\ln(1/\kappa)}\left(-\frac{\partial p}{\partial z}\right) R^2 - \frac{u_{w1}-u_{w2}}{\ln(1/\kappa)}\right] \frac{1}{r} \tag{3}$$

where η is the constant viscosity and $(-\partial p/\partial z)$ is the imposed pressure gradient. It is also clear that the slip velocities obey the slip equation, i.e.

$$\tau_{rz}(\kappa R) = F(u_{w1}) \quad \text{and} \quad \tau_{rz}(R) = -F(u_{w2}). \tag{4}$$

Substituting into Eq. (3) and after some little algebra, one finds that u_{w1} and u_{w2} satisfy the following two equations:

$$\frac{1}{2}(1-\kappa^2)\left(-\frac{\partial p}{\partial z}\right) R = \kappa F(u_{w1}) + F(u_{w2}) \tag{5}$$

and

$$\frac{2\eta}{R}(u_{w1} - u_{w2}) = \kappa F(u_{w1}) + F(u_{w2}) - \frac{2\kappa \ln(1/\kappa)}{1-\kappa^2}\left[F(u_{w1}) + \kappa F(u_{w2})\right]. \tag{6}$$

Integrating the velocity given by Eq. (2) over the annular cross section and substituting the pressure gradient from Eq. (5) lead to the following general expression for the volumetric flow-rate:

$$Q = \pi R^2 \left[u_{w2} - \kappa^2 u_{w1} + \frac{1}{2}\frac{1-\kappa^2}{\ln(1/\kappa)}(u_{w1} - u_{w2})\right] + \frac{\pi}{4\eta} R^3 \left[1 + \kappa^2 - \frac{1-\kappa^2}{\ln(1/\kappa)}\right]\left[\kappa F(u_{w1}) + F(u_{w2})\right]. \tag{7}$$

2.1. Linear slip

Let us assume that the slip equation is linear, i.e.

$$\tau_w = F(u_w) = \beta u_w \tag{8}$$

where β is a known slip parameter. Substituting into Eq. (6) and solving for u_{w2}, one gets

$$u_{w2} = \alpha u_{w1} \tag{9}$$

where

$$\alpha = \frac{(2/A) - \kappa + ((2\kappa \ln(1/\kappa))/(1-\kappa^2))}{(2/A) + 1 - ((2\kappa^2 \ln(1/\kappa))/(1-\kappa^2))} \tag{10}$$

and A is a dimensionless slip number defined by

$$A \equiv \frac{\beta R}{\eta}. \tag{11}$$

The variation of α with the radii ratio is illustrated in Fig. 2 for various values of the slip number. It turns out that $\alpha < 1$, which implies that the outer slip velocity, u_{w2}, is always smaller than the inner slip velocity, u_{w1}. As κ approaches unity, u_{w2} approaches u_{w1}, which is expected, since for small $(1-\kappa)$ the flow is equivalent to the plane Poiseuille flow, in which the velocity profile is symmetric. Moreover, in the limit of full slip ($A = 0$), $\alpha = 1$ and the velocity profile is flat.

Substituting Eqs. (8) and (9) into Eqs. (5) and (7) leads to

$$\frac{1}{2}(1-\kappa^2)\left(-\frac{\partial p}{\partial z}\right) R = \beta(\kappa+\alpha)u_{w1} \tag{12}$$

and

$$Q = \pi(1-\kappa^2)R^2 u_{w1}\left\{\frac{\alpha-\kappa^2}{1-\kappa^2} + \frac{1}{2}\frac{1-\alpha}{\ln(1/\kappa)} + \frac{A}{4}\left[\frac{1+\kappa^2}{1-\kappa^2} - \frac{1}{\ln(1/\kappa)}\right](\kappa+\alpha)\right\}. \tag{13}$$

Combining the above two equations we get the generalized Hagen–Poiseuille equation:

$$Q = \frac{\pi}{2\eta}R^4\left(-\frac{\partial p}{\partial z}\right)(1-\kappa^2)\left\{\frac{\alpha-\kappa^2}{A(\alpha+\kappa)} + \frac{(1-\kappa^2)(1-\alpha)}{2A(\alpha+\kappa)\ln(1/\kappa)} + \frac{1}{4}\left[1+\kappa^2 - \frac{1-\kappa^2}{\ln(1/\kappa)}\right]\right\}. \tag{14}$$

Scaling lengths by R, the velocity by the mean velocity V in the annulus, and the pressure by $\eta V/R$, and using stars to denote the dimensionless variables, we find that

$$u^*_{w1} = \left\{\frac{\alpha-\kappa^2}{1-\kappa^2} + \frac{1-\alpha}{2\ln(1/\kappa)} + \frac{A(\kappa+\alpha)}{4}\left[\frac{1+\kappa^2}{1-\kappa^2} - \frac{1}{\ln(1/\kappa)}\right]\right\}^{-1}. \tag{15}$$

and

$$u^*_{w2} = \alpha u^*_{w1}. \tag{16}$$

The dimensionless pressure gradient and the axial velocity profile can be calculated in terms of u^*_{w1} as follows:

$$\left(-\frac{\partial p}{\partial z}\right)^* = 2A\frac{\kappa+\alpha}{1-\kappa^2}u^*_{w1} \tag{17}$$

and

$$u^*_z(r) = u^*_{w1}\left\{\alpha - \frac{1-\alpha}{\ln(1/\kappa)}\ln r^* + \frac{A(\kappa+\alpha)}{2(1-\kappa^2)} \times \left[1 - r^{*2} + \frac{1-\kappa^2}{\ln(1/\kappa)}\ln r^*\right]\right\}. \tag{18}$$

The dependence of u^*_{w1} on κ is illustrated in Fig. 3 for various values of A. In Fig. 4 representative velocity profiles for $\kappa = 0.1$ and 0.5 are plotted. As already mentioned, the outer slip velocity is always smaller than the inner slip velocity. For $A = \infty$, $u^*_{w1} = u^*_{w2} = 0$ and the well-known velocity profiles corresponding to no slip are obtained. In the other extreme, for $A = 0$ (full slip), $u^*_{w1} = u^*_{w2} = 1$ and the velocity profiles are flat.

In order to construct dimensionless flow curves, i.e. plots of the pressure gradient versus the volumetric flow-rate, an arbitrary velocity scale (instead of the mean velocity in the annulus) is employed. Moreover, for the sake of simplicity, stars are dropped

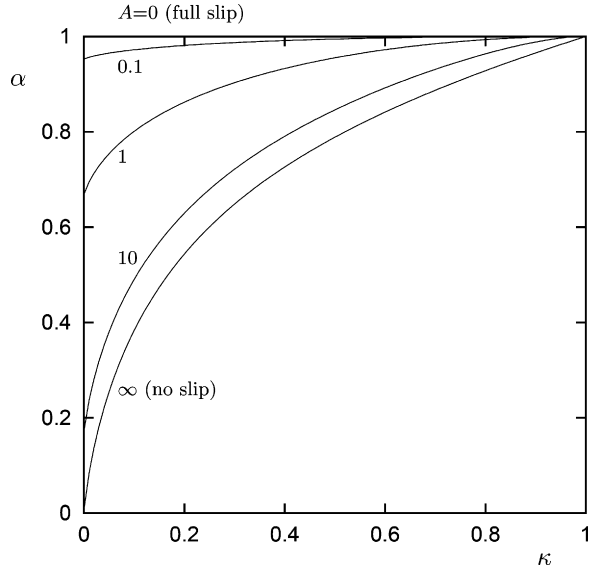

Fig. 2. Variation of α for various values of the slip number A (linear slip).

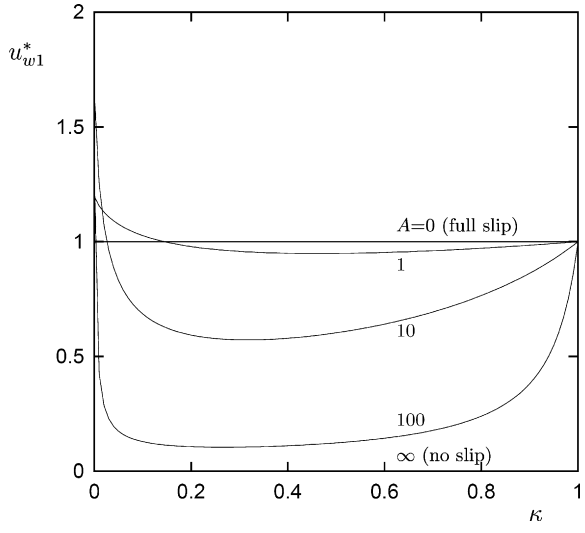

Fig. 3. The dimensionless slip velocity u^*_{w1} for various values of the slip number A (linear slip).

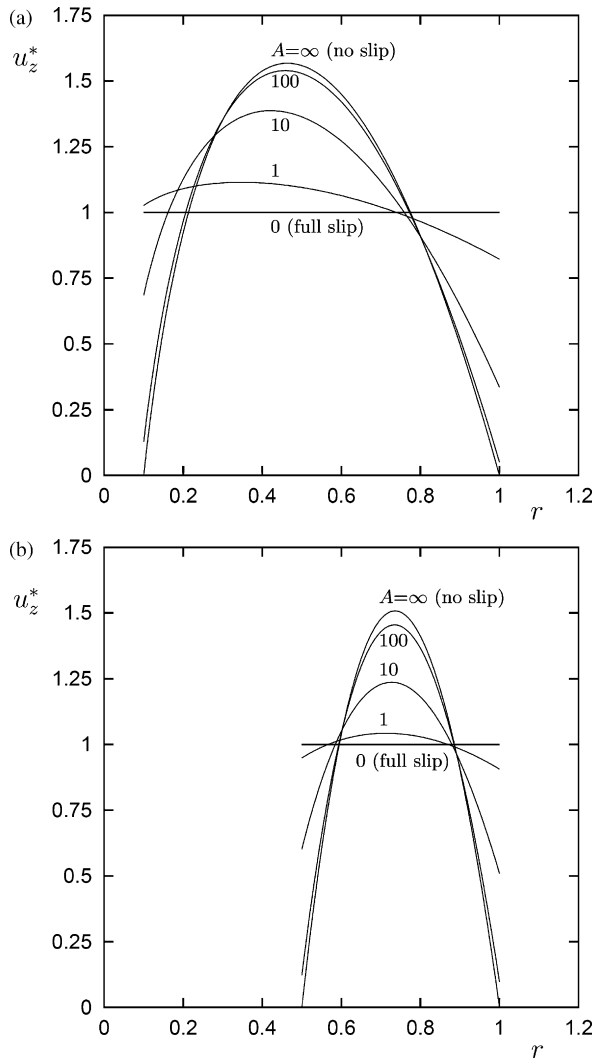

Fig. 4. Dimensionless velocity profiles for (a) $\kappa = 0.1$ and (b) $\kappa = 0.5$ and various values of the slip number A (linear slip).

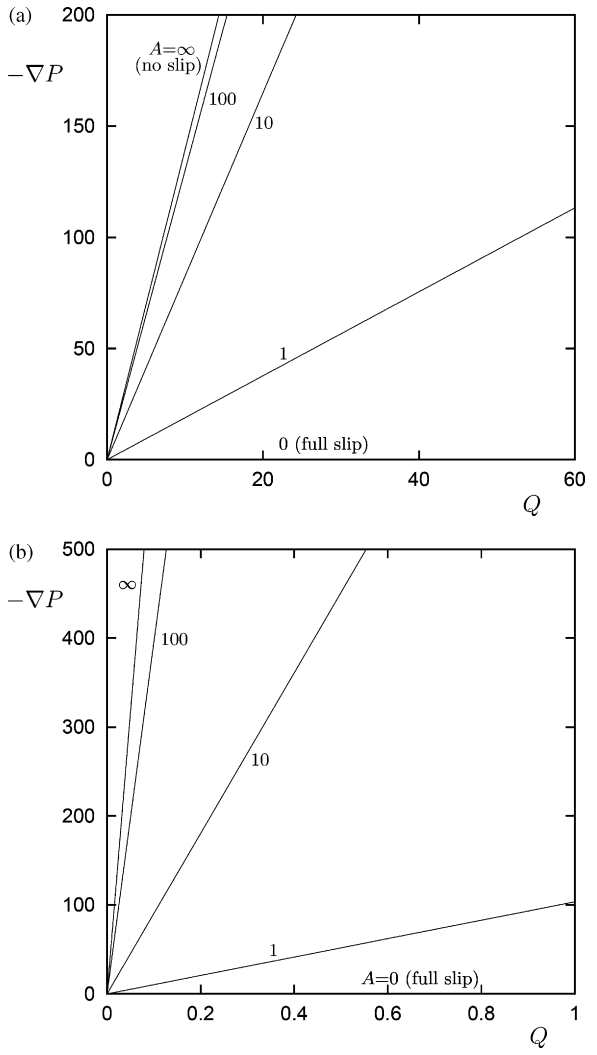

Fig. 5. The pressure gradient versus the volumetric flow-rate in the case of linear slip for (a) $\kappa = 0.1$ and (b) $\kappa = 0.9$.

hereafter. From Eq. (14) we find that

$$\left(-\frac{\partial p}{\partial z}\right) = \frac{Q/(1-\kappa^2)}{[(\alpha-\kappa^2)/(A(\alpha+\kappa))] + [((1-\kappa^2)(1-\alpha))/(2A(\alpha+\kappa) \times \ln(1/\kappa))] + [(1/4)(1+\kappa^2 - \{(1-\kappa^2)/\ln(1/\kappa)\})]} \tag{19}$$

The flow curves for different slip numbers and $\kappa = 0.1$ and 0.9 are given in Fig. 5. Naturally, the slope of the flow curve increases with A (as slip is reduced) and κ (as the annular gap is reduced). In a log–log plot (Fig. 6) the flow curves are parallel lines of slope 1 which are translated to the left as A and/or κ are increased.

2.2. Non-monotonic slip

Let us consider a generic non-monotonic slip equation with a maximum followed by a minimum, as shown in Fig. 7. It is well known that solutions with slip velocities corresponding to the negative-slope regime of the slip equation are linearly unstable and associated with the stick–slip instability [1,12,14]. Hence, when at least one of the two slip velocities is in the unstable regime, the steady-state solutions of annular Poiseuille flow are unstable.

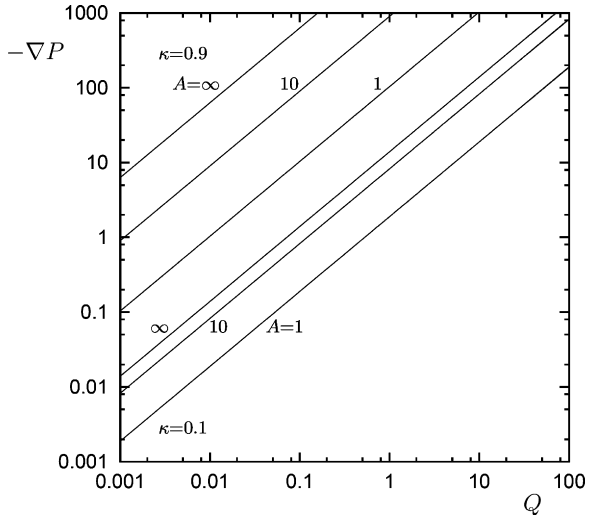

Fig. 6. Flow curves for $\kappa = 0.1$ and 0.9 in the case of linear slip.

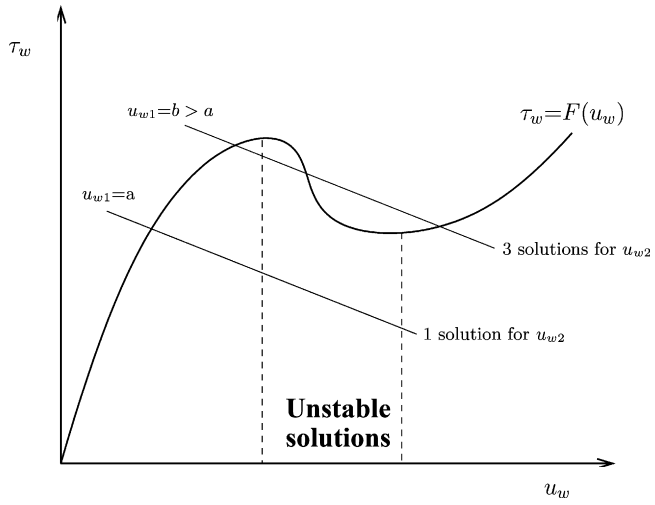

Fig. 7. Multiple steady-state solutions in the case of a non-monotonic slip equation. When the inner slip velocity u_{w1} is specified, then the outer slip velocity u_{w2} is the intersection of the slip equation and the straight line defined by Eq. (22).

Let us also assume that the inner slip velocity u_{w1} is given. From the dimensionless form of Eq. (6), one can then easily deduce that

$$\tau_{w2} = F(u_{w2}) = \frac{[2\ln(1/\kappa) - 1 + \kappa^2]\kappa F(u_{w1}) + 2(1-\kappa^2)(u_{w1} - u_{w2})}{1 - \kappa^2 - 2\kappa^2 \ln(1/\kappa)} \tag{20}$$

In other words, u_{w2} can be found as the intersection of the slip function:

$$\tau = F(u_w) \tag{21}$$

and the straight line:

$$\tau = \frac{[2\ln(1/\kappa) - 1 + \kappa^2]\kappa F(u_{w1}) + 2(1-\kappa^2)(u_{w1} - u_w)}{1 - \kappa^2 - 2\kappa^2 \ln(1/\kappa)} \tag{22}$$

which is of the negative slope:

$$-m = -\frac{2(1-\kappa^2)}{1 - \kappa^2 - 2\kappa^2 \ln(1/\kappa)} \tag{23}$$

(recall that u_{w1} is given). Hence for certain values of u_{w1} and κ there might be three solutions for u_{w2}, as illustrated in Fig. 7. If u_{w1} is in the unstable regime, then all three steady-states are unstable. Otherwise, only one of the three steady-states is unstable.

We will consider two different cases of non-monotonic three-branch slip equations, referred to here as (slip) Models 1 and 2. Model 1 is the simplest possible piecewise linear slip equation involving a minimal number of material parameters:

$$\tau_w = \begin{cases} A_1 u_w, & 0 \le u_w \le u_1 \\ A_1 u_1 + \dfrac{A_2 u_2 - A_1 u_1}{u_2 - u_1}(u_w - u_1), & u_1 \le u_w \le u_2 \\ A_2 u_w, & u_2 \le u_w \end{cases} \tag{24}$$

where A_1 and A_2 are the slip numbers corresponding to the two positive-slope branches and u_1 and u_2 define the range of the negative-slope branch of the slip equation, as illustrated in Fig. 8.

Model 2 is the non-monotonic three-branch slip equation employed by Georgiou and co-workers [19,20] based on the experimental data of Hatzikiriakos and Dealy [21]. The notation of the latter authors is kept here for this piecewise power-law slip model:

$$u_w = \begin{cases} \alpha_1 \tau_w^{m_1}, & 0 \le u_w \le u_{c2} \\ \alpha_3 \tau_w^{m_3}, & u_{c2} \le u_w \le u_{\min} \\ \alpha_2 \tau_w^{m_2}, & u_w \ge u_{\min} \end{cases}. \tag{25}$$

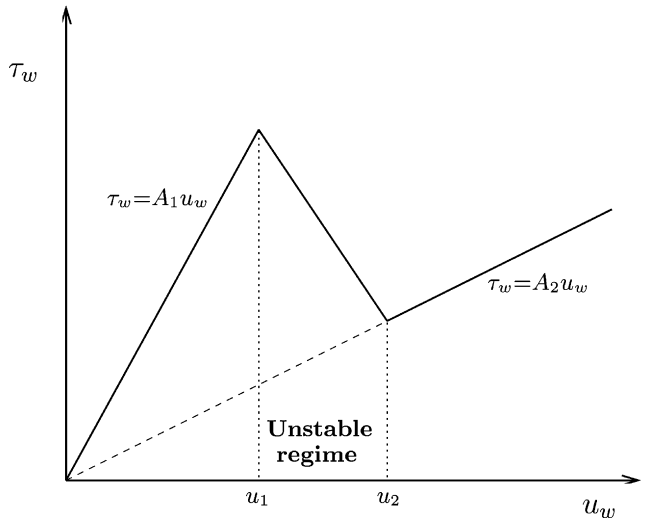

Fig. 8. The piece-wise linear non-monotonic slip equation (Model 1).

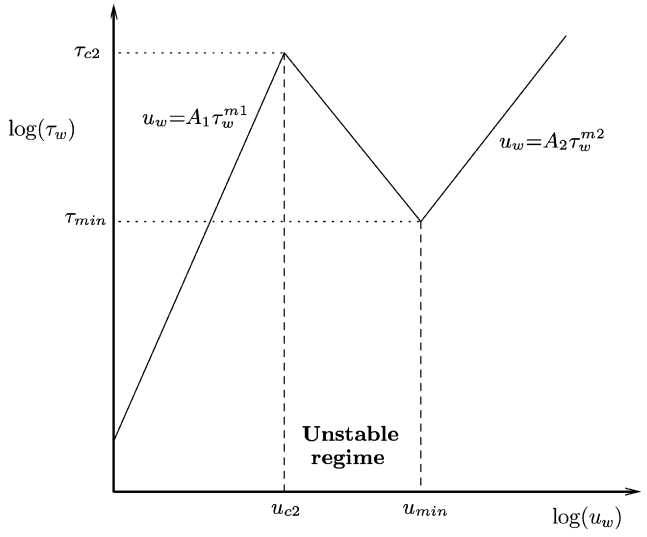

Fig. 9. The non-monotonic three-branch slip Model 2 (log–log plot).

The difference of Model 2 from Model 1 is that the three branches are straight segments in a log–log plot instead of a linear plot, as illustrated in Fig. 9, where some of the model parameters are also defined. The left positive-slope branch results from the slip equation Hatzikiriakos and Dealy [21] proposed for the left branch of their flow curve after substituting all parameters and taking the normal stress as infinite. The right positive-slope branch is the power-law slip equation suggested by the same researchers for the right branch of their flow curve. Finally, the negative-slope branch,

Table 1
Values of the parameters in the original non-monotonic slip Model 2.

Parameter	Value
α_1 ((MPa)$^{-m1}$ cm/s)	125.09
m_1	3.23
α_2 ((MPa)$^{-m2}$ cm/s)	1000
m_2	2.86
α_3 ((MPa)$^{-m3}$ cm/s)	5.484×10^{-3}
m_3	−4.434
τ_{c2} (MPa)	0.27
$\tau_{\min}$ (MPa)	0.19
v_{c2} (cm/s)	1.82
$v_{\min}$ (cm/s)	8.65

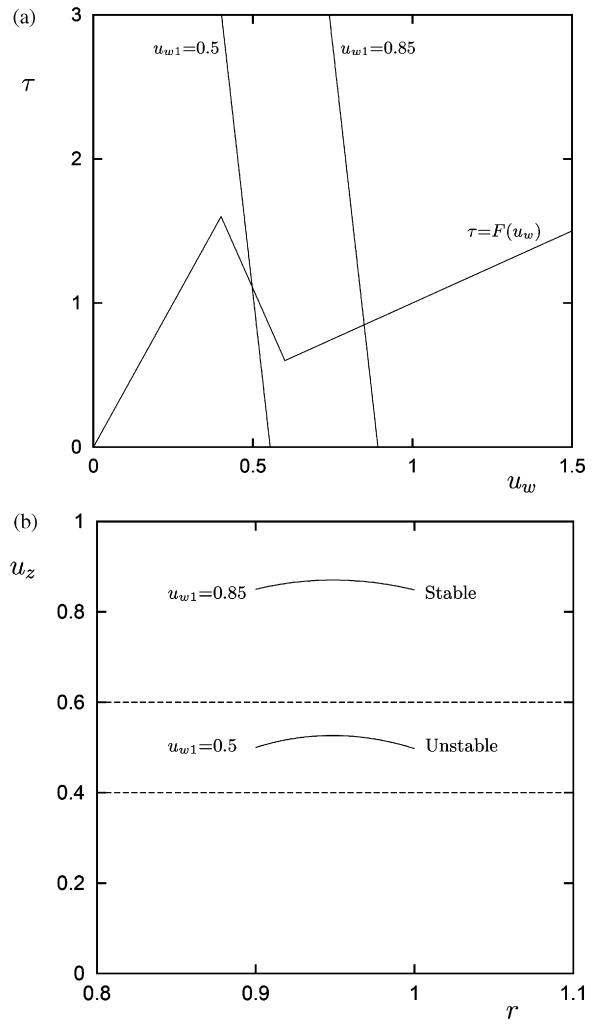

Fig. 10. Steady-state solutions for $\kappa = 0.9$ with the piecewise linear slip Model 1: (a) the unique solutions for u_{w2} when $u_{w1} = 0.5$ and 0.85 are found as the intersections of the straight lines defined by Eq. (22) with the slip equation; (b) the corresponding velocity profiles. The dashed lines show the unstable regime for wall slip velocities; $A_1 = 4$, $A_2 = 1$, $u_1 = 0.4$ and $u_2 = 0.6$.

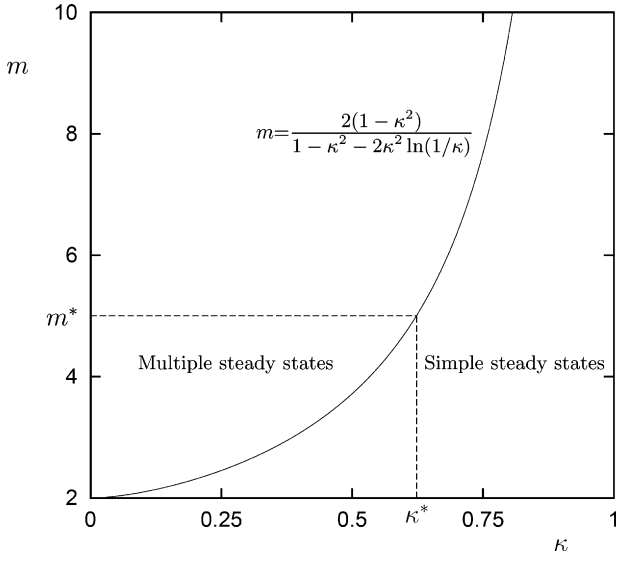

Fig. 11. Regimes of multiple and simple steady states with the piecewise linear slip Model 1; $A_1 = 4$, $A_2 = 1$, $u_1 = 0.4$ and $u_2 = 0.6$.

which corresponds to the unstable region of the flow curve for which no measurements have been possible, is just the straight line connecting the other two branches in a log–log plot. Thus,

$$m_3 = \frac{\ln\left(u_{c2}/u_{\min}\right)}{\ln\left(\tau_{c2}/\tau_{\min}\right)} \quad \text{and} \quad a_3 = \frac{u_{c2}}{\tau_{c2}^{m_3}}.$$

The dimensionless form of Eq. (25) is

$$u_{\mathrm{w}} = \begin{cases} A_1\tau_{\mathrm{w}}^{m_1}, & 0 \le u_{\mathrm{w}} \le u_{c2} \\ A_3\tau_{\mathrm{w}}^{m_3}, & u_{c2} \le u_{\mathrm{w}} \le u_{\min} \\ A_2\tau_{\mathrm{w}}^{m_2}, & u_{\mathrm{w}} \ge u_{\min} \end{cases}. \tag{26}$$

The dimensionless numbers that appear in this equation are defined as follows:

$$A_i \equiv \frac{a_i\eta^{m_i}V^{m_i}}{R^{m_i}}, \quad i = 1, 2, 3, \tag{27}$$

and the dimensionless values of u_{c2} and $u_{\min}$ correspond to

$$\tau_{c2}^* \equiv \frac{\tau_{c2}R}{\eta V} \quad \text{and} \quad \tau_{\min}^* \equiv \frac{\tau_{\min}R}{\eta V}, \tag{28}$$

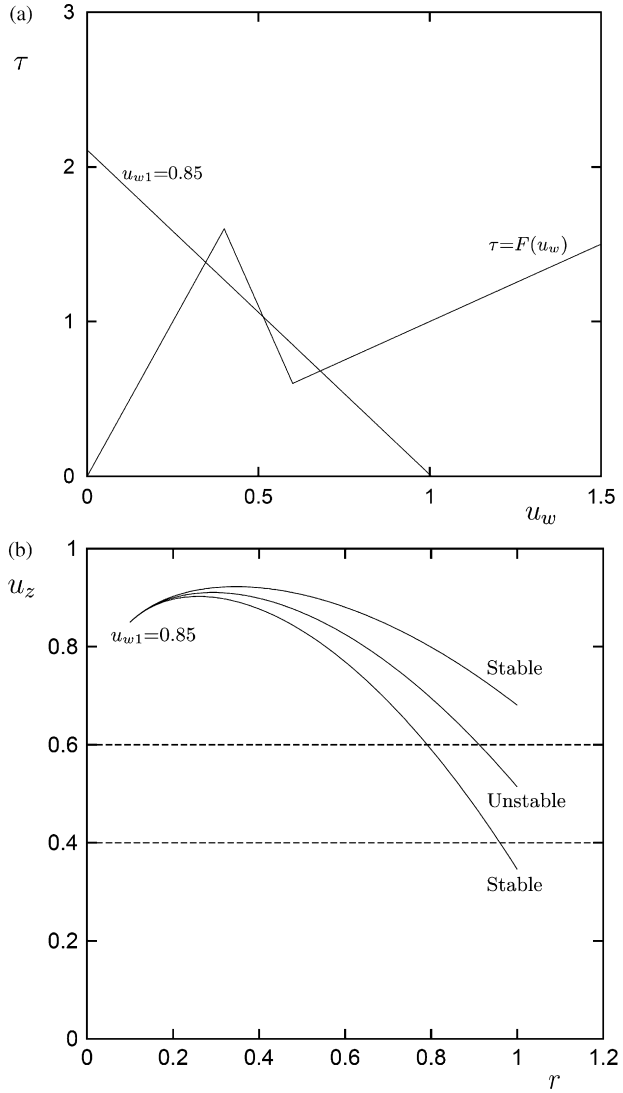

Fig. 12. Multiple steady-state solutions for $\kappa = 0.1$ with the piecewise linear slip Model 1: (a) the three solutions for u_{w2} when $u_{w1} = 0.85$ are found as the intersections of the straight line defined by Eq. (22) and the slip equation; (b) the corresponding velocity profiles. The dashed lines show the unstable regime for wall slip velocities; $A_1 = 4$, $A_2 = 1$, $u_1 = 0.4$ and $u_2 = 0.6$.

respectively. The dimensional parameters of the above slip equation are given in Table 1.

3. Numerical results

In order to study the phenomena caused by non-monotonic slip, we first considered the piecewise linear slip Model 1 with $A_1 = 4$, $A_2 = 1$, $u_1 = 0.4$ and $u_2 = 0.6$. Recall that steady-states with one or both slip velocities in the interval (0.4, 0.6) are linearly unstable. As explained below, in the case of annuli with a small gap, e.g. with $\kappa = 0.9$, there are no multiple solutions. In Fig. 10 a, we plot slip Model 1 with the straight lines defined by Eq. (22) when $u_{w1} = 0.5$ and 0.85. Since there are no multiple solutions, the straight lines intersect the slip equation once. The unique velocity profiles for the two values of u_{w1} are shown in Fig. 10 b. The first is unstable, since the two slip velocities, u_{w1} and u_{w2}, are in the unstable regime of the slip equation, whereas the second velocity profile is stable.

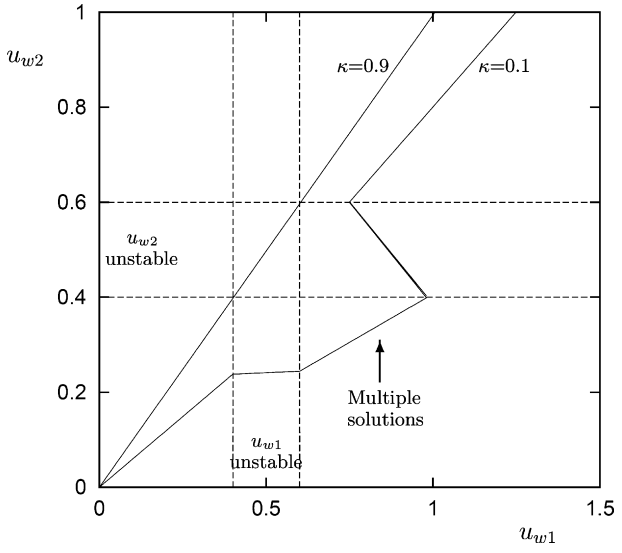

Fig. 13. The outer slip velocity u_{w2} as a function of the inner slip velocity u_{w1} calculated using the piecewise linear slip Model 1 with $A_1 = 4$, $A_2 = 1$, $u_1 = 0.4$ and $u_2 = 0.6$. The dashed lines show the unstable regime for wall slip velocities.

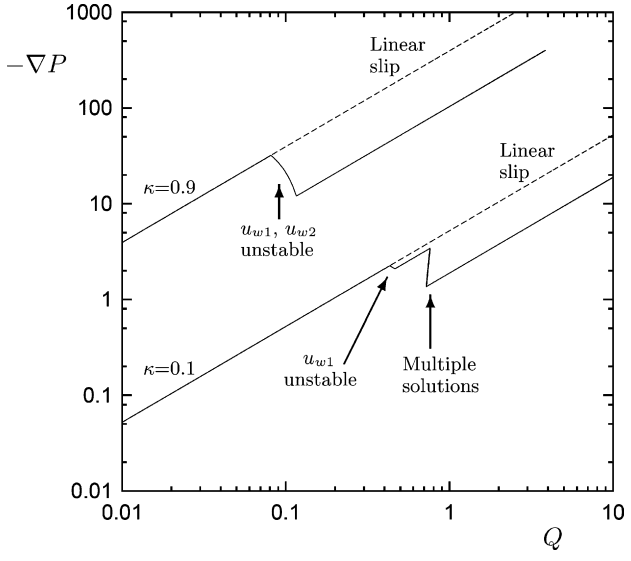

Fig. 14. Flow curves for $\kappa = 0.1$ and 0.9 obtained using the piecewise linear Model 1 with $A_1 = 4$, $A_2 = 1$, $u_1 = 0.4$ and $u_2 = 0.6$. The dashed lines show the flow curves in the case of linear slip with $A = A_1 = 4$.

In both cases, slip is so strong that the velocity profiles are almost plug.

It is easily deduced that a necessary and sufficient condition for having multiple steady states in the case the negative-slope branch of a non-monotonic slip equation is a straight line of slope $-m^*$ is $m^* > m$, where m is the slope of the straight line defined by Eq. (22). Hence, the critical radii ratio κ^* below which multiple solutions are admissible is the solution of

$$m^* = \frac{2(1-\kappa^{*2})}{1-\kappa^{*2}-2\kappa^{*2}\ln(1/\kappa^*)}. \tag{29}$$

As illustrated in Fig. 11, multiple steady states exist only for low values of the radii ratio (below κ^*). Moreover, since $m \geq 2$, if the slope of the unstable branch of the slip equation is less than 2, there exist no multiple solutions, irrespective the value of κ. It should be noted that in the extreme, practically unattainable case when $\kappa = \kappa^*$ and u_{w1} assumes a certain theoretical value, the straight line defined by Eq. (22) coincides with the negative-slope branch of the piecewise linear slip equation, which implies the existence of infinitely many unstable (and thus not observable) steady-state solutions. In Fig. 12 we present results obtained with $\kappa = 0.1$. For $u_{w1} = 0.85$ (i.e. for a stable value of the inner slip velocity) there exist three possible solutions for u_{w2}, only one of which falls in the unstable regime (Fig. 12a). The two stable as well as the unstable velocity profiles are shown in Fig. 12 b.

In Fig. 13, the inner slip velocity u_{w1} is plotted versus the outer slip velocity u_{w2} for both $\kappa = 0.1$ and 0.9. It is observed that for high values of κ the plot is a straight line and both the inner and outer slip velocities (which are close to each other) fall in the unstable regime almost simultaneously, since the velocity profile is almost symmetric. This is expected, since as $\kappa \to 1$, the plane Poiseuille flow is approached in which the velocity profile is symmetric. At reduced values of κ the velocity profile is more asymmetric so that u_{w2} is stable for all values of u_{w1} in the unstable regime. More importantly, the range of u_{w2} values corresponding to unstable u_{w1} is rather narrow, which implies that the range of volumetric flow-rates corresponding to such solutions is narrow as well. It is also clear that in a range of higher values of u_{w1}, there correspond three solutions for u_{w2}, of which only one is unstable.

The above observations have direct impact on the flow curves, which are given in Fig. 14. For high values of κ, due to the non-monotonicity of the slip equation, there exists a rather wide unstable regime in which the slope of the flow curve is negative,

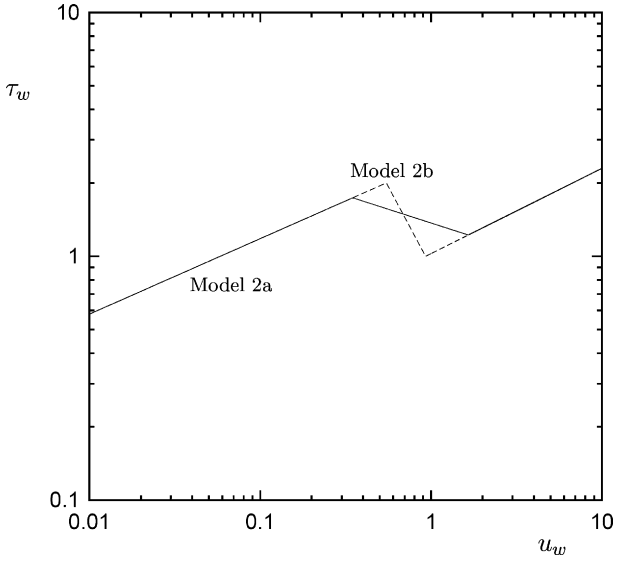

Fig. 15. Non-monotonic slip Models 2a and 2b.

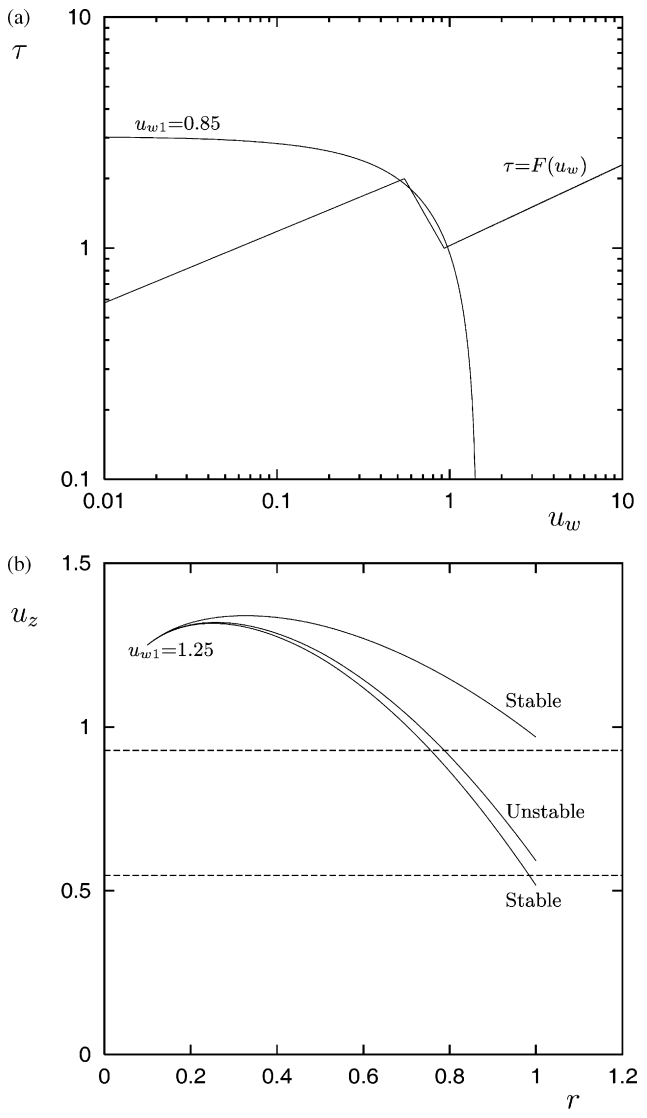

Fig. 16. Multiple steady-state solutions for $\kappa = 0.1$ with the non-monotonic slip Model 2b: (a) the three solutions for u_{w2} when $u_{w1} = 1.25$ are found as the intersections of the straight line defined by Eq. (22) and the slip equation; (b) the corresponding velocity profiles. The dashed lines show the unstable regime for wall slip velocities.

i.e. a stick–slip regime. For low values of κ, however, we observe that the negative-slope regime of the flow curve is rather narrow. This corresponds to steady velocity profiles in which only u_{w1} lies in the unstable regime of the slip equation. At a higher regime of volumetric flow-rates, to the same stable value of u_{w1} there correspond three steady-states. Since only one of these solutions is unstable, one of the two stable solutions is observed in practice, and, hence, this regime is considered stable. Therefore, when non-monotonic piecewise linear slip occurs along the walls and κ is below a critical value, there exists only a very narrow instability regime in the flow curve, which may not be observed in practice. The size of this regime is reduced further by reducing κ. As shown below, a second instability regime may appear if the negative-slope branch of the slip equation is not linear. This corresponds to a regime where u_{w1} is stable and only one unstable solution for u_{w2} is allowed.

Let us now proceed to the results obtained with the more realistic slip Model 2. In addition to the original model, a modified version with a narrower unstable range and a steeper negative-slope branch has also been employed, by using different values of the critical wall shear stresses τ_{min} and τ_{c2} and keeping the slopes of the two stable branches constant. The original and the modified versions of the model, referred to respectively as Models 2a and 2b, are plotted in Fig. 15. The corresponding values of the dimensionless parameters are tabulated in Table 2.

Table 2
Dimensionless parameters of non-monotonic slip Models 2a and 2b.

Dimensionless number	Model 2a	Model 2b
m_1	3.23	3.23
A_1	0.0583	0.0583
m_2	2.86	2.86
A_2	0.929	0.929
m_3	−4.43	−4.43
A_3	4.04	4.04
τ_{c2}	1.738	2
τ_{min}	1.223	1

As already discussed, with slip equations exhibiting a maximum and a minimum three steady-state solutions are allowed in a certain range of volumetric flow-rates. Such a case is illustrated in Fig. 16 a, where slip Model 2b is used with $u_{w1} = 1.25$ and $\kappa = 0.1$. The three velocity profiles are shown in Fig. 16 b. It should be noted

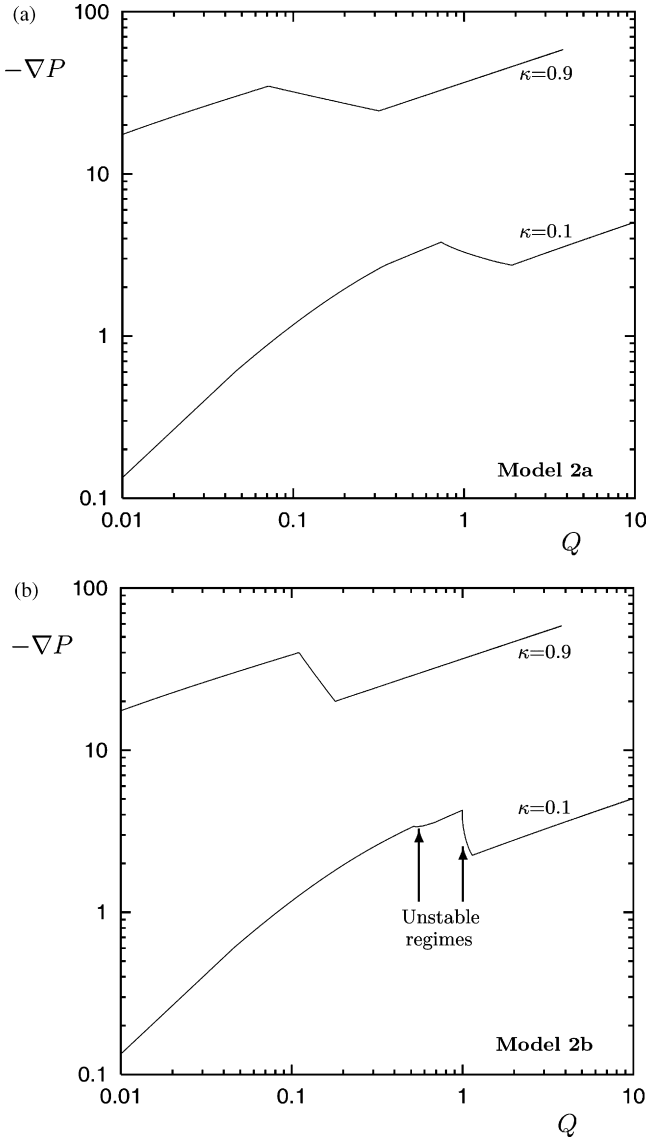

Fig. 17. Flow curves for $\kappa = 0.1$ and 0.9 obtained with the non-monotonic slip Models 2a and 2b.

that the intermediate solution is linearly unstable, since the outer slip velocity u_{w2} corresponds to the negative-slope regime of the slip equation [12,14].

In Fig. 17 we give the calculated flow curves for $\kappa = 0.1$ and 0.9 using Models 2a and 2b. No multiple solutions have been obtained with Model 2a irrespective of the value of κ. The corresponding flow curves are characterized by a stick–slip regime the size of which is reduced as κ is decreased. With Model 2b, however, multiple solutions are admitted below a critical value of κ, e.g. for $\kappa = 0.1$. For this particular case, there are two narrow stick–slip regimes, due to the nonlinearity of the negative-slope branch of the slip equation. In the first regime u_{w1} falls into the unstable regime and in the second u_{w2} is unstable while u_{w1} is stable; in both cases, the unstable solutions are unique. By comparing all curves, one can conclude that the size of the unstable regime is reduced as κ is reduced. The instability regime is much smaller in the case of Model 2b, which proved to admit multiple steady-state solutions. Our calculations indicated that the range of multiple steady states increases as the radii ratio κ is reduced. As κ is reduced the stick–slip regimes move to the right (i.e. to higher flow rates) and their sizes are reduced. These observations may explain, at least partially, the fact that the stick–slip instability is not observed in annular extrusion experiments.

4. Conclusions

The annular Poiseuille flow of a Newtonian fluid has been studied assuming that slip occurs along the walls. In addition to the standard linear slip equation, two non-monotonic slip equations exhibiting a maximum and a minimum, have also been considered. Due to the asymmetry of the velocity profile the slip velocities at the inner and outer cylinders of the annulus are not the same. The shape of the flow curve depends on the radii ratio, κ, and the form of the slip equation. The flow curve is always monotonic in the case of linear slip. Using a non-monotonic slip equation results in a non-monotonic flow curve with one or two narrow unstable negative-slope branches that correspond to the stick–slip extrusion instability regime.

In general, when κ is relatively high, the flow curve exhibits a negative-slope stick–slip branch which corresponds to steady-state solutions with at least one of the two slip velocities being in the unstable regime of the slip equation. This stick–slip instability regime is shifted to the right and its size is reduced as κ is decreased. For low values of κ, the flow curve may exhibit two narrow negative-slope branches. The first of them corresponds to steady-state solutions with unstable inner slip velocity and stable outer slip velocity, while in the second one the opposite is true. Again, the sizes of the two unstable regimes are reduced as κ is decreased. It has been demonstrated that for certain non-monotonic slip equations multiple steady states are allowed below a critical value of κ. More specifically, to a given stable value of the inner slip velocity there correspond three values of the outer slip velocity, only one of which is in the unstable regime. Due to the existence of the other two stable steady-state solutions, the second stick–slip instability regime may be eliminated and the flow curve may exhibit only a vertical jump. These observations may explain the absence of the stick–slip instability in annular extrusion experiments when κ is small.

In the present study, we have considered the Newtonian flow in order to demonstrate more clearly the effects of slip. In a more realistic simulation of the stick–slip instability, using a generalized-Newtonian or a viscoelastic constitutive equation will be more appropriate. An interesting question that arises is whether there exists a selection mechanism for the two stable steady-states when the corresponding unstable steady-state is perturbed. This is the subject of our current investigations.

References

[1] G. Georgiou, The stick–slip instability, in: S.G. Hatzikiriakos, K. Migler (Eds.), Polymer Processing Instabilities: Control and Understanding, Marcel Dekker Inc, New York, 2004, pp. 161–206, Chapter 6.
[2] S.G. Hatzikiriakos, K. Migler (Eds.), Polymer Processing Instabilities: Control and Understanding, Marcel Dekker Inc., New York, 2004.
[3] L. Robert, B. Vergnes, Y. Demay, Flow birefringence study of the stick–slip instability during extrusion of high-density polyethylenes, J. Non-Newton. Fluid Mech. 112 (2003) 27–42.
[4] C. Combeaud, B. Vergnes, A. Merten, D. Hertle, H. Münstedt, Volume defects during extrusion of polystyrene investigated by flow induced birefringence and laser-Doppler velocimetry, J. Non-Newton. Fluid Mech. 145 (2007) 69–77.
[5] E.E. Rosenbaum, Rheology and processability of FEP Teflon resins for wire coating, PhD Thesis, University of British Columbia, 1998.
[6] E.E. Rosenbaum, S. Randa, S.G. Hatzikiriakos, C.W. Stewart, D.L. Henry, M. Buckmaster, Boron nitride as a processing aid for the extrusion of polyolefins and fluoropolymers, Polym. Eng. Sci. 40 (2000) 179–190.
[7] O. Delgadillo-Velàzquez, G. Georgiou, M. Sentmanat, S.G. Hatzikiriakos, Sharkskin and oscillating melt fracture: why in slit and capillary dies and not in annular dies? Polym. Eng. Sci. 48 (2008) 405–414.
[8] G. Karapetsas, J. Tsamopoulos, Steady extrusion of viscoelastic materials from an annular die, J. Non-Newton. Fluid Mech. 154 (2008) 136–152.
[9] A. Garcia-Rejon, R.W. DiRaddo, M.E. Ryan, Effect of die geometry and die characteristics on viscoelastic annular swell, J. Non-Newton. Fluid Mech. 60 (1995) 107–128.
[10] E. Mitsoulis, Annular extrudate swell of pseudoplastic and viscoplastic fluids, J. Non-Newton. Fluid Mech. 141 (2007) 138–147.
[11] M.M. Denn, Extrusion instabilities and wall slip, Annu. Rev. Fluid Mech. 33 (2001) 265–287.
[12] J.R.A. Pearson, Mechanics of Polymer Processing, Elsevier, London, 1985.
[13] G.C. Georgiou, On the stability of the shear flow of a viscoelastic fluid with slip along the fixed wall, Rheol. Acta 35 (1996) 39–47.
[14] E. Brasseur, M.M. Fyrillas, G.C. Georgiou, M.J. Crochet, The time-dependent extrudate-swell problem of an Oldroyd-B fluid with slip along the wall, J. Rheol. 42 (1998) 549–566.
[15] N. El Kissi, J.-M. Piau, Écoulement de fluides polymères enchevêtrés dans un capillaire. Modélisation du glissement macroscopique à la paroi, C. R. Acad. Sci. Paris, Sér. II 309 (1989) 7–9.
[16] K.E.P. Adewale, A.I. Leonov, Modeling spurt and stress oscillations in flows of molten polymers, Rheol. Acta 36 (1997) 110–127.
[17] J.M. Piau, N. El Kissi, Measurement and modelling of friction in polymer melts during macroscopic slip at the wall, J. Non-Newton. Fluid Mech. 54 (1994) 121–142.
[18] J.L.A. Dubbeldam, J. Molenaar, Dynamics of the spurt instability in polymer extrusion, J. Non-Newton. Fluid Mech. 112 (2003) 217–235.
[19] E. Taliadorou, G.C. Georgiou, A.N. Alexandrou, A two-dimensional numerical study of the stick–slip extrusion instability, J. Non-Newton. Fluid Mech. 146 (2007) 30–44.
[20] G. Georgiou, The time-dependent compressible extrudate-swell flows of Carreau fluid with slip at the wall, J. Non-Newton. Fluid Mech. 109 (2003) 93–114.
[21] S.G. Hatzikiriakos, J.M. Dealy, Role of slip and fracture in the oscillating flow of HDPE in a capillary, J. Rheol. 36 (1992) 845–884.